Redox chemistry, solubility and hydrolysis of Re in reducing aquatic systems. Thermodynamic description and comparison with Tc

S. Duckworth [a,*], X. Gaona [a,**], D. Castaño [a], S. Park [b,1], M. Altmaier [a], H. Geckeis [a]

[a] KIT-INE Karlsruhe Institute of Technology - Institute for Nuclear Waste Disposal in Karlsruhe, Gemany
[b] Kyung Hee University, Department of Nuclear Engineering, Seoul, Republic of Korea

Handling editorProf. M. Kersten

Keywords:
Rhenium
Redox
Solubility
Hydrolysis
Kinetics
Thermodynamics

A B S T R A C T

The aqueous solution chemistry of rhenium was investigated in acidic to hyperalkaline reducing systems buffered by Sn(II) and $Na_2S_2O_4$. Oversaturation experiments with $[NaReO_4]_0 = 10^{-3}$ M were used to evaluate the redox chemistry of Re(VII)/Re(IV), whereas the solubility and hydrolysis of Re(IV) were investigated in a series of undersaturation experiments with ReO_2(s).

The predominance of Re(IV) is predicted under the very reducing conditions defined by Sn(II) and $Na_2S_2O_4$ (at $pe + pH_m \approx 1$–5) (with $pH_m = -\log [H^+]$ and $pe = -\log a_{e^-}$), according to thermodynamic calculations represented as *Pourbaix* diagrams. In contrast to Tc(VII), Re(VII) shows recalcitrance to the reduction in Sn(II) systems except at $pH_m \approx 1$ and ≈12.8. As previously reported in the literature, the reduction of Re(VII) observed at $pH_m \approx 1$ is expectedly triggered by the co-precipitation of Re(IV) with the SnO_2(s) solid phase forming through the *in-situ* oxidation of Sn(II). The faster reduction kinetics reported for Tc(VII) can be partly explained by the more positive standard potential (E°) of the couple TcO_4^-/TcO_2(s) compared to that of ReO_4^-/ReO_2(s), which results in a greater driving force for the reduction of TcO_4^- under the same conditions.

The solubility of ReO_2(s) remains low (≈10^{-6} M) and pH-independent within $1 \leq pH_m \leq 10$, but increases with a slope of +1 (log [Re] *vs.* pH_m) above $pH_m \approx 10$. A combination of solid phase characterization, solubility data determined in this work and reported in the literature are considered to derive chemical and thermodynamic models including the solubility reactions $ReO_2(s) + H_2O(l) \Leftrightarrow ReO(OH)_2(aq)$ and $ReO_2(s) + 2H_2O(l) \Leftrightarrow ReO(OH)_3^- + H^+$. Thermodynamic data determined in this work for the hydrolysis of Re(IV) show a good agreement with thermodynamic data reported for Tc(IV), and represent a significant improvement with respect to previous studies available on the Re (IV) system.

Experimental evidence obtained in this work support the chemical analogy of Re and Tc in the +IV oxidation state, which is rationalized by the very similar ionic radii of both metal ions. Notwithstanding, these elements show a remarkably different redox chemistry, both in terms of kinetics and thermodynamic stability. The use of Re as an inactive analogue of Tc in systems involving redox transformations must therefore be considered with precaution.

1. Introduction

Rhenium (Z 75) belongs to the group VIIB of the periodic table, together with manganese (Z 25), technetium (Z 43) and bohrium (Z 107). It is one of the less abundant elements in the earth's crust, with an estimated abundance between 0.7 and 1 ppb (Anderson et al., 2013; Millensifer, 2010; Naumov, 2007) and compared to the elements in its group it is considered a non-toxic metal. Rheniite (ReS_2) is the only reported mineral of rhenium (Korzhinsky et al., 1994; Tessalina et al., 2008), which otherwise is usually found associated with molybdenum-copper porphyry deposits (Woolf, 1961). Rhenium is characterized by one of the highest melting points of any metal in the periodic table (3180 °C), which explains its main application in the production of heat-resistant alloys used in both aerospace and industrial

* Corresponding author.
** Corresponding author.
E-mail addresses: sarah.duckworth@kit.edu (S. Duckworth), xavier.gaona@kit.edu (X. Gaona).
[1] Current address: Division of Advanced Nuclear Engineering (DANE), Pohang University of Science and Technology (POSTECH), Pohang, Gyeongbuk, Republic of Korea.

gas-fired turbines (Anderson et al., 2013; Naumov, 2007). Since its first applications during the 70s in petrochemical catalysts, the use of rhenium within this industrial field has steadily increased (Anderson et al., 2013; Lwin and Wachs, 2014; Mol, 1999; Naumov, 2007).

Re is often considered as a chemical analogue of Tc, whose ^{99}Tc isotope is one of the main long-lived fission products ($t_{1/2}$ 2.13 × 10^5 years) produced in nuclear reactors and thus present in spent nuclear fuel. Re and Tc are characterized by similar electronic configurations (Re: [Xe] $4f^{14}$ $5d^5$ $6s^2$; Tc: [Kr] $4d^5$ $5s^2$), with up to seven electrons in the outer shell. Complexes with oxidation states ranging from +I to + VII have been described for both elements. In aqueous systems and in the absence of complexing ligands, the most stable oxidation states of both Re and Tc are + IV and +VII. The sparingly soluble hydrous oxides ReO_2(s, hyd) and TcO_2(s, hyd) prevail under reducing conditions, whereas the highly soluble ReO_4^- and TcO_4^- control the aquatic chemistry of these elements in oxidizing systems. Re and Tc in their oxidation states + IV and +VII are characterized by very similar ionic radii ($r_{Re^{4+}}$ 0.63 Å *vs.* $r_{Tc^{4+}}$ 0.65 Å, $r_{Re^{7+}}$ 0.53 Å *vs.* $r_{Tc^{7+}}$ 0.56 Å, all with coordination number (CN) of 6, or $r_{Re^{7+}}$ 0.38 Å *vs.* $r_{Tc^{7+}}$ 0.37 Å with CN 6) (Shannon, 1976), which partially explains the similar behavior of both elements in aqueous systems. In spite of this, relevant differences arise when involving redox transitions, in particular for the couple MO_4^-/MO_2(s), for which the standard potentials E° 0.510 and 0.746 V have been reported for Re and Tc, respectively (Grenthe et al., 2020; Woolf, 1961).

The solubility and hydrolysis of Re(IV) has been far less investigated compared to its Tc(IV) counterpart. Kim et al. studied the solubility of ReO_2(s) and Re_2O_3(s) under oxic and anoxic conditions (Kim and Boulègue, 2003). The authors concluded that Re_2O_3(s) is not stable within the investigated conditions, whereas ReO_2(s) was reported to control the solubility of Re in anoxic systems with 2 ≤ pH ≤ 9. The pH-independent behavior observed in this pH region was attributed to the equilibrium reaction ReO_2(s) + H_2O(l) ⇔ $ReO(OH)_2$(aq), although the authors proposed also the formation of the anionic species $ReO(OH)_3^-$ above pH ≈ 8. We note that analogous hydrolysis species have been reported to play a key role in the aqueous chemistry of Tc in reducing system, even though the formation of $TcO(OH)_3^-$ has been described to take place at significantly higher pH values, *i.e.* above pH ≈ 10.5 (Baumann et al., 2017; Grenthe et al., 2020; Yalçıntaş et al., 2016). Khan and co-workers investigated the chemical reduction of Re (VII) by Sn(II) at pH ≈ 1.4 under air (Khan et al., 2018). Under these conditions, the authors reported the incorporation of reduced Re(IV) into the SnO_2(s) lattice structure. Solubility experiments conducted with the co-precipitated Sn(Re)O_2(s) phase and with ReO_2(s) under air showed a more recalcitrant behavior of the former, thus highlighting the additional stabilization of Re(IV) gained through the incorporation into the SnO_2(s) structure. Xiong and Wood investigated the solubility of ReO_2(s) in 0.5–1.5 m KCl solutions at t 500 °C using different oxide pairs as oxygen fugacity buffers (Co–CoO, Ni–NiO, Re–ReO_2, MnO–Mn_3O_4, and MoO_2–MoO_3) (Xiong and Wood, 1999). The authors reported the predominance of Re in the oxidation state + IV, with a small fraction of dissolved Re possibly found in the +V or higher oxidation state. Based on the very important increase in solubility observed with increasing chloride concentration, the authors concluded on the relevant role of Re(IV)–Cl complexes within the investigated conditions. The same research group studied the solubility of Re within 100 and 200 °C and the oxygen fugacity buffered by fixing the partial pressure of hydrogen gas (Xiong et al., 2006; Xiong and Wood, 2001). The authors reported the predominance of the neutral species Re$(OH)_4$(aq) (or $ReO(OH)_2$(aq)) within 2.2 ≤ pH ≤ 8.8, and provided a temperature-dependent expression for the calculation of the equilibrium constant of the solubility reaction ReO_2(s) + 2 H_2O(l) ⇔ Re$(OH)_4$(aq) at t 25–200 °C. Poineau et al. investigated the electrochemical reduction of Re(VII) and Tc(VII) in HCl media (Poineau et al., 2006). UV–vis and XAFS measurements confirmed that the reduction of Re(VII) in 4.0 M HCl results in the formation of chlorinated species, possibly $ReCl_6^{2-}$, $ReCl_5(OH)^{2-}$ and $Re_2OCl_{10}^{4-}$. In contrast to Re, the reduction of Tc(VII) in very acidic conditions resulted in a Tc(IV)/Tc(III) mixture. Rulfs and Meyer investigated the solubility of K_2ReCl_6(s), K_2ReBr_6(s) and K_2ReI_6(s) in 1 M of the corresponding hydrohalide acids (Rulfs and Meyer, 1955). In the same work, the authors studied the hydrolysis of $ReCl_6^{2-}$ by means of potentiometric titrations. Based on their observations, Rulfs and Meyer reported the formation of the cationic species Re$(OH)_3(H_2O)_3^+$ prior to the precipitation of ReO_2(s).

In this context, this work aims at a comprehensive investigation of the redox chemistry of Re(VII)/Re(IV), as well as the solubility and hydrolysis of Re(IV) in reducing systems. For this purpose, systematic oversaturation experiments with $[NaReO_4]_0$ 10^{-3} M and undersaturation solubility experiments with ReO_2(s) are performed in 0.1 M NaCl solutions with 1 ≤ pH_m ≤ 12.8 (with pH_m –log $[H^+]$). Together with an extensive solid phase characterization, these experiments allow a complete thermodynamic description of the Re(IV) aqueous system in the absence of complexing ligands and moderate background electrolyte concentrations. Kinetic and thermodynamic considerations obtained in this work are used to discuss the analogies and differences with the Tc system.

2. Experimental

2.1. Chemicals

Sodium chloride (NaCl, p. a.), nitric acid (65%) (HNO_3, Suprapure) and sodium dithionite anhydrous ($Na_2S_2O_4$, ≥87%) were obtained from Merck. Rhenium dioxide (ReO_2, 99.7%), Sodium perrhenate ($NaReO_4$, 99.99%) and tin(II) chloride ($SnCl_2$, 98%) were purchased from Sigma-Aldrich. Ethanol (99.9%) was obtained from VWR Chemicals.

Purified water (Millipore Milli-Q Advantage A10 (18.2 MΩ cm at 25 °C, 4 ppb TOC) with Millipore Millipak® 40 0.22 μm) purged with Ar for at least 1 h to remove traces of oxygen was used for sample preparation. Handling and preparation of all samples was performed in an Ar glovebox with <3 ppm O_2 at t (22 ± 2) °C.

For the measurement of the pH, the pH electrode was calibrated using pH standard buffer solutions (pH 2 to 10) from Merck. To adjust the pH of the samples, sodium hydroxide (NaOH, Titrisol® Merck) or hydrochloric acid (HCl, Titrisol® Merck) were used.

2.2. pH_m and E_h measurements

The proton concentration (pH_m log$[H^+]$, $[H^+]$ in molal units (m mol kg_w^{-1})) was measured using a ROSS combination pH electrode (Thermo Scientific, Orion™) calibrated against standard buffer solutions as indicated above. In aqueous solutions with ionic strength I_m ≥ 0.1 m, the measured pH value (pH_{exp}) is an operational apparent value related to the molal proton concentration $[H^+]$ by pH_m pH_{exp} + A_m. The empirical correction factor A_m entails both the liquid junction potential of the electrode as well as the activity coefficient of $[H^+]$. A_m values for sodium chloride systems are well known and have been previously reported in the literature (Altmaier et al., 2003).

E_h measurements were conducted using a Pt combination electrode (Metrohm) with Ag/AgCl as a reference system. The measured redox potentials were converted to E_h *vs.* SHE (standard hydrogen electrode) by correcting for the potential of the Ag/AgCl reference electrode (+207 mV for 3 M KCl at 25 °C). For the E_h measurements all samples were stirred continuously for 25 min during the measurement. In analogy to the pH value, the apparent electron activity (pe log a_e) was calculated from pe 16.9 E_h [V], according to the equation E_h $\frac{RT\ \ln(10)}{F}$ pe.

The accuracy of the redox electrode was tested with a standard redox buffer solution (+220 mV vs. Ag/AgCl, Schott), which provided readings within ±10 mV of the certified value.

2.3. Redox and solubility experiments

The redox chemistry of Re under reducing conditions was investigated in a series of oversaturation experiments with $[NaReO_4]_0$ 10^{-3} M. The reduction of Re(VII) to Re(IV) is expected to result in the sparingly soluble $ReO_2(s)$, with the consequent decrease of the initial Re concentration. Note that the starting Re(VII) concentration (10^{-3} M) is significantly higher than analogous redox experiments performed with Tc(VII) (10^{-5} M) (Kobayashi et al., 2013; Yalçıntaş et al., 2015). The initial Re(VII) concentration in the present study was selected on the basis of solubility data obtained by Kim and co-workers for $ReO_2(s)$ (Kim and Boulègue, 2003), who reported Re(IV) concentrations in equilibrium with this solid phase about two orders of magnitude higher than the Tc(IV) counterpart (Yalçıntaş et al., 2016).

All samples (redox and solubility) were prepared at constant ionic strength as defined by 0.1 M NaCl with $1.0 \leq pH_m \leq 12.8$. Experiments were carried out in Zinsser vials (HDPE, Polyvials®, Zinsser Analytic) with 15 mL of background solution. The pH_m of the samples was adjusted with HCl–NaCl or NaOH–NaCl solutions of the same ionic strength. Reducing conditions were imposed with 0.01 M Sn(II) (added to the samples as solid $SnCl_2$) or 0.01 M $Na_2S_2O_4$.

Undersaturation solubility experiments with commercial $ReO_2(s)$ (*ca.* 4 mg per sample) were performed under analogous reducing conditions. Experimental solubility data obtained for this system can be directly compared with undersaturation solubility data reported by Yalçıntaş and co-workers for $TcO_2{\cdot}0.6H_2O(am)$ under similar experimental conditions (Yalçıntaş et al., 2016).

Background solutions including reducing chemicals were equilibrated for 14 d (days) in an Ar-glovebox, and pH_m and E_h values were monitored until stable pH_m (±0.05 of the targeted value) values and the necessary reducing conditions were attained. After reaching stable pH_m and E_h readings, $NaReO_4$ was added directly and dissolved in the oversaturation redox experiments. In the undersaturation solubility experiments, about 4 mg of the purified $ReO_2(s)$ solid phase were washed three times with 1 mL of the respective matrix solution and then added to 15 mL of the same matrix solution. The concentration of rhenium after 10 kD ultrafiltration (Omega™, 2–3 nm cut-off, Nanosep®, Pall Life Science), pH_m and E_h were measured at regular time intervals for up to 352 d. The Re concentration was quantified by ICP-OES (inductively coupled plasma optical emission spectrometry, Perkin Elmer Optima 8300DV) for the samples with $[Re] \geq 10^{-4}$ M (oversaturation redox samples) and by ICP-MS (inductively coupled plasma mass spectrometry, Thermo Scientific™ iCAP™ TQs) for the samples with $[Re] < 10^{-4}$ M (mostly undersaturation solubility samples). The uncertainty for the ICP-OES measurements was 5% and for the ICP-MS device the uncertainty lies between 5 and 10%. For the preparation of the ICP-OES/MS samples, 500 μL of the supernatant solution were centrifuged in polypropylene tubes equipped with 10 kD filters for 5 min at 13500 rpm (12225 *g*) to separate possible colloidal or suspended solid phase particles. Aliquots of the obtained solutions were diluted with 2% HNO_3 and subsequently measured.

2.4. Solid phase characterization

After attaining equilibrium conditions, the solid phases were characterized by X-ray diffraction (XRD): (i) solid phases precipitated in the oversaturation redox experiments with $NaReO_4$ at pH_m 1.0, 6.2, 10.5, 11.4 and 12.8 in the presence of Sn(II), and (ii) with $ReO_2(s)$ in the undersaturation solubility experiments at pH_m 3.4, 9.5, 11.5, 12.8 in the presence of Sn(II), and at pH_m 12.8 with $Na_2S_2O_4$. For each of the investigated samples, an aliquot of approximately 1–2 mg of the Re solid-phase was washed five times with 1 mL of ethanol inside an Ar-glovebox, in order to completely remove the salt-containing matrix, which can interfere in the characterization of the Re solid. After the last washing step, the solid phase was suspended in ≈30 μL of ethanol and transferred to a capped silicon single crystal sample holder (Dome, Bruker). After the evaporation of the ethanol, the sample was taken out of the glovebox and the XRD patterns were collected on a Bruker AXS D Advance X-ray powder diffractometer. Measurements were performed at angles 2θ 2–80° with incremental steps of 0.02–0.04° and accumulation time of 1 s per step. The resulting diffraction patterns were compared with powder diffraction files (PDF) provided by the JCPDS-ICDD database (Wong-Ng et al., 2001).

3. Results and discussion

3.1. Pourbaix diagrams and experimental (pe + pH_m) measurements

Fig. 1 shows the *Pourbaix* diagram of Re in dilute aqueous NaCl solution at $[Re]_{tot}$ 10^{-3} M, calculated for $0 \leq pH_m \leq 14$ and $15 \leq pe \leq 15$ using thermodynamic data extracted from (Kim and Boulègue, 2003) and summarized in Table 1. Note that although the authors calculated solubility and *Pourbaix* diagrams using thermodynamic data derived from their own solubility experiments (Figures 6 to 8 in Kim and Boulègue, 2003), the corresponding equilibrium constants were not provided in the paper. However, the diagrams reported by the authors allow to properly extract the solubility and hydrolysis constants provided in Table 1.

Fig. 1 also includes the (pe + pH_m) values measured for the redox (oversaturation conditions) and solubility (undersaturation conditions) experiments in the presence of Sn(II) or $Na_2S_2O_4$ as reducing agents. The dark blue lines in Fig. 1 represent a 1:1 distribution of the redox couple Re(VII)/Re(IV) according to reaction (1), whereas the black dotted lines represent the calculations involving only aqueous species of Re(VII) and Re(IV).

$$ReO_4^- + 4\,H^+ + 3\,e^- \Leftrightarrow ReO_2(s) + 2\,H_2O \quad (1)$$

Experimentally measured (pe + pH_m) values determined in both redox and solubility experiments lie well below the calculated Re(VII)/

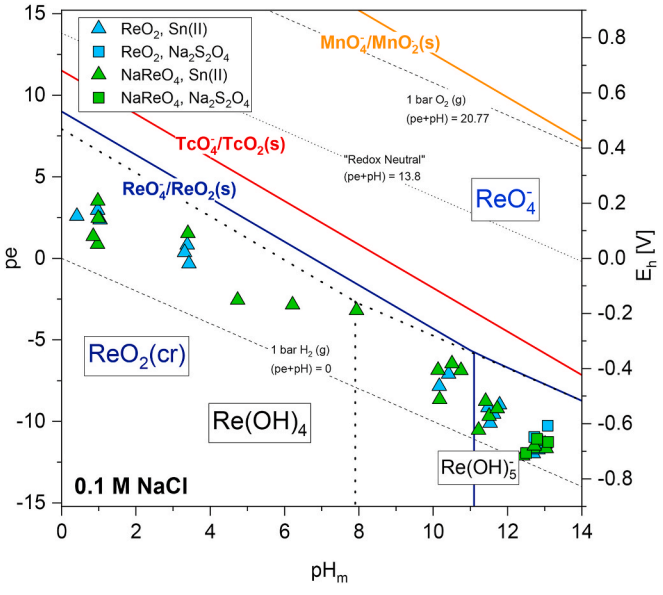

Fig. 1. Experimentally measured pe and pH_m values in NaCl solutions with I = 0.1 M (note that very low or high pH_m exceed this ionic strength). The values of pe and pH_m are plotted in the Pourbaix diagram of Re calculated at I = 0.1 and $[Re]_{tot} = 10^{-3}$ M using the thermodynamic data extracted from (Kim and Boulègue, 2003) and summarized in Table 1. Solid lines in blue, red and green correspond to the redox borderline $MO_4^- + 4\,H^+ + 3\,e^- \Leftrightarrow MO_2(s) + 2\,H_2O(l)$ for M = Re, Tc and Mn, respectively (see section 3.2 for details). Calculations are conducted with the code Spana (Puigdomènech et al., 2014). (For interpretation of the references to colour in this figure legend, the reader is referred to the Web version of this article.)

Table 1
Solubility and hydrolysis constants determined in the present work for Re(IV), and reported in the literature for Re(IV) and analogous Tc(IV) systems.

Reaction	log K° (Re)	log K° (Tc)	Reference
$MO_2{\cdot}xH_2O(s) + (1\text{-}x)\ H_2O(l) \quad MO(OH)_2(aq)$	–(6.3 ± 0.3)		This work
	–6.2[a]		Kim and Boulègue (2003)
		–(8.80 ± 0.50)	Yalçıntaş et al. (2016)
		–(7.66 ± 1.22)[b]	Grenthe et al. (2020)
		–(8.72 ± 0.40)[c]	Grenthe et al. (2020)
$2MO(OH)_2(aq) + 2\ H^+ \quad M_2O_2(OH)_2^{2+} + 2\ H_2O(l)$	–	(12.99 ± 0.41)	Grenthe et al. (2020)
$3MO(OH)_2(aq) + 2\ H^+ \quad M_3O_5^{2+} + 4\ H_2O(l)$	–	(21.81 ± 1.5)	Yalçıntaş et al. (2016)
$MO(OH)_2(aq) + H_2O(l) \quad MO(OH)_3^- + H^+$	**–(10.7 ± 0.3)**		**This work**
	–8[a]		Kim and Boulègue (2003)
		–(10.47 ± 0.06)	Yalçıntaş et al. (2016)
		–(10.92 ± 0.17)	Grenthe et al. (2020)
$MO_4 + 4\ H^+ + 3\ e \Leftrightarrow MO_2(s) + 2\ H_2O(l)$	29.94[d]	(37.83 ± 0.61)	(Kim and Boulègue, 2003) in (Puigdomènech et al., 2014)
			Grenthe et al. (2020)

[a] Equilibrium constants are not explicitly reported by Kim and Boulègue (2003). The values summarized in this table have been extracted from the Pourbaix diagram shown in Figure 6 of (Kim and Boulègue, 2003).
[b] Solubility constant corresponding to TcO_2(am, hyd, fresh), selected on the basis of solubility data at $t < 24$ d.
[c] Solubility constant corresponding to TcO_2(am, hyd, aged), selected on the basis of solubility data at $t \geq 24$ d.
[d] Equilibrium constants in the database distributed with the software Spana described in (Puigdomènech et al., 2014), with (Kim and Boulègue, 2003) as the reported reference. The software Spana was downloaded on October 7th, 2019.

Re(IV) redox borderline. The redox potential slightly increased over time (≤352 d), especially in the samples with Sn(II) as reducing agent. However, all (pe + pH_m) values are still below the Re(VII)/Re(IV) redox borderline after this equilibration time, indicating that both Sn(II) and $Na_2S_2O_4$ are capable to maintain reducing conditions over the investigated timeframe. During the relatively long equilibration time for the experiments, oxygen from the glove box has the possibility to constantly diffuse through the HDPE walls of the vials, but the amount of reductants used was enough to scavenge the traces of oxygen. Note further that the (pe + pH_m) values measured in this work are in line with data previously reported for analogous reducing systems (Baumann et al., 2017; Kobayashi et al., 2013; Yalçıntaş et al., 2015, 2016) prepared in order to study the Tc(VII)/Tc(IV) couple.

The comparison of experimental (pe + pH_m) values with thermodynamic calculations in the form of a Pourbaix diagram predict that (under equilibrium conditions) Re should be found in the reduced + IV state in all samples investigated in this work. In all systems up to $pH_m \approx 11$, thermodynamic calculations also predict the predominant precipitation/stabilization of ReO_2(s). However, due to the formation of the anionic species $ReO(OH)_3^-$ above $pH_m \approx 8$ with the consequent increase in the solubility of ReO_2(s), a full dissolution of the solid phase and predominance of $ReO(OH)_3^-$ is expected (according to thermodynamic calculations) for the samples prepared at $pH_m \approx 12$ and 12.8.

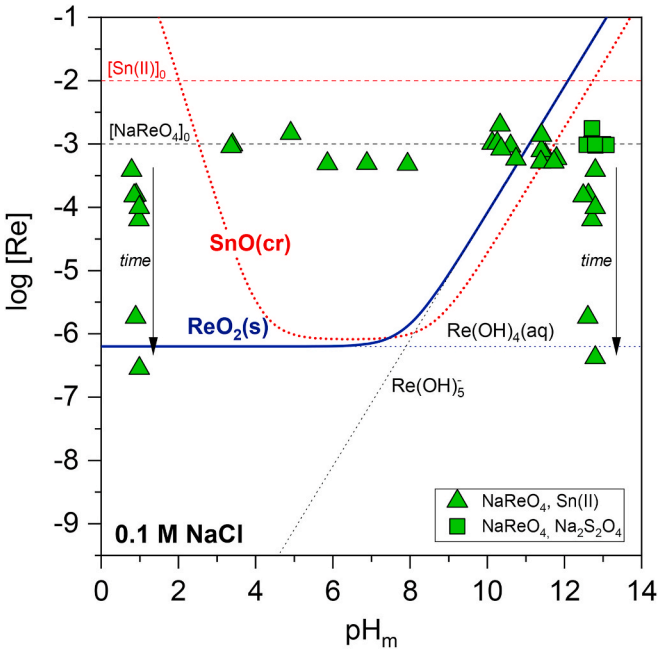

Fig. 2. Aqueous concentrations of Re measured in the redox experiments with $[NaReO_4]_0 = 10^{-3}$ M in the presence of Sn(II) and $Na_2S_2O_4$ as reducing agents. Systems equilibrated for $t \leq 352$ d. Solid blue line correspond to the solubility of ReO_2(s) calculated using the thermodynamic data extracted from (Kim and Boulègue, 2003) and summarized in Table 1. The bold dashed red line shows the solubility of SnO(cr), as calculated using thermodynamic data reported in (Gamsjäger et al., 2012). Horizontal dashed lines indicate the initial concentrations of $NaReO_4$ (black line) and Sn(II) (red line). (For interpretation of the references to colour in this figure legend, the reader is referred to the Web version of this article.)

3.2. Redox behavior of Re in acidic to hyperalkaline reducing systems

Fig. 2 shows the total concentrations of Re measured in the redox experiments with $[NaReO_4]_0 \quad 10^{-3}$ M in the presence of Sn(II) and $Na_2S_2O_4$ and equilibrated for up to 352 d. For comparison purposes, the figure also shows the solubility of ReO_2(s) calculated using the thermodynamic data extracted from (Kim and Boulègue, 2003) and summarized in Table 1.

Fig. 2 shows that no significant decrease in the concentration of rhenium takes place for the samples within $3 \leq pH_m \leq 12$. In these cases, the entire added Re(VII) inventory was dissolved and then remained stable in solution for 352 d. However, in the Sn(II) systems with the lowest and highest pH_m (≈1 and ≈12.8) the formation of a solid phase accompanied by a clear decrease in the Re concentration is observed after 307 d. This observation suggests the reduction of the original dissolved Re(VII) to Re(IV) and the subsequent precipitation of ReO_2(s). In contrast, the measurements of (pe + pH_m) in combination with thermodynamic equilibrium calculations predict the reduction of Re(VII) to Re(IV) in all the oversaturation samples (see section 3.1), which is not observed experimentally. Such discrepancy is attributed to the slow reduction kinetics often encountered for multielectron transitions as the one under investigation, Re(VII) → Re(IV). The different reduction kinetics observed for Re(VII) as a function of pH can be correlated with the availability of Sn(II) in solution. Hence, Sn(II) is characterized by the formation of the sparingly soluble hydroxide Sn $(OH)_2$(s) and by an amphoteric behavior, showing the highest Sn concentrations in solution in very acidic (predominance of Sn^{2+} and $SnOH^+$) and hyperalkaline (predominance of $Sn(OH)_3^-$) conditions (see dashed red curve in Fig. 2).

In a previous study dedicated to the redox chemistry of Re, Khan et al. reported the fast reduction of Re(VII) by Sn(II) under oxic acidic conditions (Khan et al., 2018). Within less than 1 day, the authors observed a decrease of 60% in the original Re(VII) concentration. The fast decrease in the initial Re concentration was correlated to the incorporation of Re(IV) into the lattice structure of the forming SnO_2(s), which is facilitated by the similar ionic radii of both metal ions ($r_{Sn^{4+}}$ 0.69 Å, $r_{Re^{4+}}$ 0.63 Å, both with coordination numbers of 6 (Shannon, 1976)). Khan and co-workers explained the incomplete reduction of Re(VII) on the basis of the ratio Sn(II): Re(VII) of 1 : 1 used in the experiments, which is below the 3 : 2 stoichiometric requirement. Indeed, Maun and Davidson reported the complete reduction of Re(VII) to Re(IV) only at Sn(II): Re(VII) ratios above 3 : 1 (Maun and Davidson, 1950).

Previous experimental studies investigating the reduction of Tc(VII) to Tc(IV) in several reducing systems also reported slow reduction kinetics (up to 400 d), although in Sn(II) systems a full reduction was observed within $t \leq 130$ d at $3 \leq pH_m \leq 12$ (Kobayashi et al., 2013; Yalçıntaş et al., 2015). Lukens and co-workers also reported a dissimilar redox behavior of technetium and rhenium in borosilicate glass melts (Lukens et al., 2007), with Re(VII) being more stable toward reduction than Tc(VII). Reinoso Maset and co-workers studied the reduction of Tc (VII) ($[TcO_4^-]_0$ $5.4{\cdot}10^{-7}$ M) and Re(VII) ($[ReO_4^-]_0$ $2.7{\cdot}10^{-7}$ M) at pH 6.2 in the presence of Sn(II) ($[Sn(II)]_0$ $5{\cdot}10^{-3}$ and 0.01 M) and different organic ligands (EDTA, NTA or ISA, with $[L]_0$ $1.3{\cdot}10^{-3}$ – $2.3{\cdot}10^{-3}$ M) (Maset et al., 2006). The authors followed the evolution of [Tc] and [Re] with time ($t \leq 42$ d), and determined the oxidation state of Tc and Re by means of HPLC-ICP-MS. The reduction of Tc(VII) to Tc(IV) was observed within less than 10 d, whereas Re remained in the +VII oxidation state within the investigated timeframe.

Our experimental observations as well as previous results reported in the literature highlight the differences in the redox behavior of Tc and Re under reducing conditions. Thermodynamic data of redox transitions for elements in the Group 7 of the periodic table are compared in Fig. 1, where solid lines in blue, red and green correspond to the redox borderline $MO_4^- + 4\ H^+ + 3\ e^- \Leftrightarrow MO_2(s) + 2\ H_2O(l)$ for M Re (Z 75), Tc (Z 43) and Mn (Z 25), respectively. This comparison clearly shows the increased stability of MO_4^- with increasing atomic number (Z). Hence, although thermodynamic calculations predict the reduction of both Tc(VII) and Re(VII) in the very reducing ($pe + pH_m$) values defined by Sn(II) systems, the driving force expressed as the difference between the thermodynamically calculated pe values and the measured pe value (Δpe $pe_{borderline} - pe_{experimental}$) is clearly greater for Tc than for Re, which can explain the faster reduction kinetics observed for the former.

We also notice in Fig. 2 that the concentration of Re decreases significantly at pH_m 13, even though literature data predict high Re (IV)-solubility due to the formation of $ReO(OH)_3^-$. This discrepancy will be further investigated and discussed in the next section.

3.3. Solubility of Re(IV) in acidic to hyperalkaline reducing systems

Fig. 3 depicts the experimental solubility data of Re(IV) determined from undersaturation conditions in 0.1 M NaCl solutions equilibrated for ≤ 352 d. The figure also shows experimental solubility data reported by Kim and Boulègue for ReO_2(s) within $1.5 \leq pH \leq 10$ (Kim and Boulègue, 2003), as well as the solubility of $TcO_2{\cdot}0.6H_2O$(am) determined by Yalçıntaş et al. in 0.1 M NaCl solutions (Yalçıntaş et al., 2016). Solid lines in the figure correspond to the solubility of ReO_2(s) and $TcO_2{\cdot}0.6H_2O$(am) calculated as described in the figure caption.

Solubility data determined in this work for Re(IV) show a pH_m-independent behavior within $1 \leq pH_m \leq 10$. These results are in excellent agreement with the solubility data reported by Kim and Boulègue, who proposed a solubility control by the equilibrium reaction $ReO_2(s) + H_2O(l) \Leftrightarrow ReO(OH)_2(aq)$ in this pH region. In spite of the amphoteric behavior predicted for Re(IV), no increase in the solubility is observed under acidic conditions. This observation is apparently in contradiction with the solubility behavior described by Yalçıntaş and co-workers for the solubility of Tc(IV) in NaCl solutions (Yalçıntaş et al., 2016). The increase in solubility observed by these authors in this pH region was attributed to the predominance of the trimeric species $Tc_3O_5^{2+}$ in equilibrium with $TcO_2{\cdot}0.6H_2O$(am). However, we note that the enhancement of the solubility was mostly observed at high background electrolyte concentrations (3 and 5 M NaCl), *i.e.* the formation of $Tc_3O_5^{2+}$ is possibly promoted by ion interaction processes. Analogous Re species might be expected at higher ionic strengths and/or lower pH values than those investigated in this work.

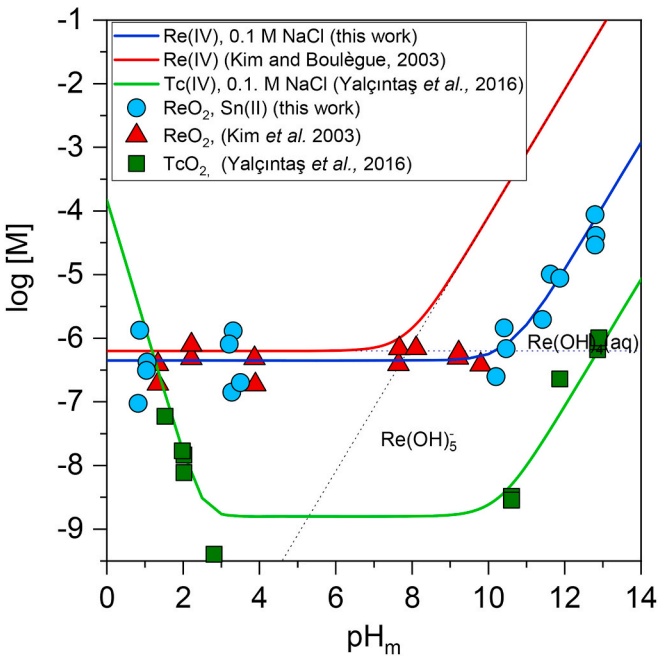

Fig. 3. Experimental solubility data for Re(IV) determined from undersaturation conditions in the present work (blue symbols) or reported in Kim and Boulègue (Kim and Boulègue, 2003) (red symbols). Green symbols show the solubility of Tc(IV) determined by Yalçıntaş et al. under analogous experimental conditions (Yalçıntaş et al., 2016). Blue and red solid lines correspond to the solubility of ReO_2(s) calculated using the thermodynamic model determined in this work or extracted from (Kim and Boulègue, 2003), respectively (see Table 1 for additional explanations). The green line represents the solubility of $TcO_2{\cdot}0.6H_2O$(am) calculated using the thermodynamic data reported in (Grenthe et al., 2020; Yalçıntaş et al., 2016). (For interpretation of the references to colour in this figure legend, the reader is referred to the Web version of this article.)

A clear increase in the solubility can be observed at $pH_m > 10$. In spite of the dispersion in the solubility data, a slope of +1 (log [Re] *vs.* pH_m) can be determined for this pH_m-region. This indicates that one H^+ is being released in the equilibrium reaction controlling the solubility under these conditions. Although with an absolute solubility about 1.5 log_{10}-units lower, the trends in the solubility data reported for Tc(IV) under hyperalkaline conditions are in excellent agreement with solubility data reported in this work for Re(IV). This observation underpins a similar hydrolysis behavior for both metal ions in the oxidation state + IV. The use of thermodynamic data extracted from Kim and Boulèque predicts the formation of the anionic species $ReO(OH)_3^-$ above

pH ≈ 8 with the consequent increase in the solubility of ReO_2(s) (solid red line in Fig. 3) (Kim and Boulègue, 2003), which is not confirmed by our study. Kim and Boulègue assumed the formation of $ReO(OH)_3^-$ based on their solubility data at pH > 9 (see red symbols in Fig. 3). The small decrease in pH observed under these conditions was attributed by the authors to the consumption of OH^- caused by the formation of the complex $ReO(OH)_3^-$. Although the explanation for the slight decrease in pH might be correct, we consider that the solubility and *Pourbaix* diagrams calculated by the authors are in gross error, as it can explain neither their own experimental data, where a solubility increase at pH_m > 8 is not visible, nor our solubility results.

3.4. Solid phase characterization

XRD patterns obtained for solid phases collected from redox (oversaturation) and solubility (undersaturation) experiments are shown in Fig. 4. Samples were equilibrated at different pH_m values ranging from pH_m ≈ 1 to 12.8. Most of the samples contained Sn(II) as reducing chemical, although $Na_2S_2O_4$ was in some cases used for comparison purposes in samples equilibrated at pH_m 12.8. Redox samples equilibrated at pH_m 6.2, 10.5 and 11.4 showed no or very minor decrease in the initial Re concentration (see section 3.2), and thus the collected diffractograms expectedly correspond to solid Sn(II) phases.

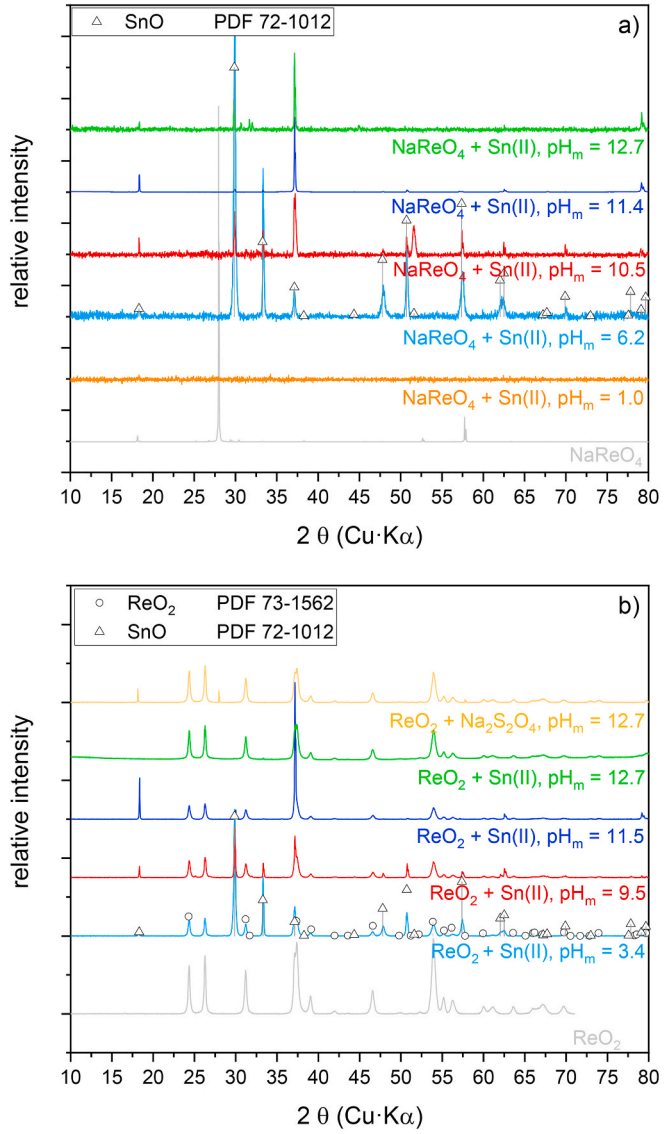

Fig. 4. XRD patterns obtained for solid phases collected from (a) redox (oversaturation) and (b) solubility (undersaturation) experiments. The grey lines correspond to the diffractograms of the starting materials $NaReO_4$ (Figure a) or ReO_2 (Figure b). Symbols - either circles or triangles - are used to indicate ReO_2 and SnO (see the corresponding legends in a and b) reference diffractograms as reported in the JCPDS-ICDD database (Gates-Rector and Blanton, 2019).

The sharp reflections observed in Fig. 4a for redox samples equilibrated in NaCl solutions at pH_m 6.2, 10.5 and 11.4 are in perfect agreement with reference data reported for SnO(cr) (PDF number 72–1012). Weaker but still clear patterns corresponding to SnO(cr) (2θ ≈ 29.9 and 37.1) are visible for the sample equilibrated at pH_m 12.7, reflecting that at this pH_m most of the Sn(II) in the system is expectedly found as soluble species. No reflections are observed for the solid phase equilibrated at pH_m ≈ 1, which indicates the amorphous character of the solid phase formed under these conditions. It is evident that according to XRD analyses pure ReO_2 is absent in the studied solid phases. In their experiments under similar conditions (pH 1.4, reduction of Re(VII) with equimolar concentration of Sn (II)), Khan and co-workers reported the incorporation of Re(IV) in the SnO_2(s) structure (Khan et al., 2018). The authors unequivocally identified the Sn(IV) solid phase on the basis of the excellent agreement of the XRD patterns with those of cassiterite, SnO_2(cr). After the co-precipitation of the Sn(Re)O_2(s) solid phase, the authors exposed the solid material to two cycles of washing and drying at 50 °C. We hypothesize that the treatment at elevated temperature may be responsible for the different crystallinity of the solid obtained by Khan et al. and in the present work. The formation of Sn(Re)O_2(s) coprecipitates in the oversaturation experiments is most likely responsible for the Re concentration at pH_m 13 being much lower than in the undersaturation study.

The main patterns observed in the diffractograms shown in Fig. 4b are consistent with the starting material and with reference data reported for ReO_2(cr) (PDF number 73–1562). The sharp reflections at 2θ ≈ 18.3, 29.9, 33.3, 37.1, 51.6, 57.4, 62.0 and 62.5 can be assigned to SnO(cr) (PDF number 72–1012). With increasing pH_m, the intensities of these reflections decrease due to increased solubilization of Sn(II) through the formation of $Sn(OH)_3^-$, and they disappear at pH_m ≈ 12.8. These results confirm that the initial material ReO_2(s) was not altered in the course of the undersaturation solubility experiments.

3.5. Thermodynamic description of the Re(IV) solubility and hydrolysis

The combination of undersaturation solubility data and solid phase characterization provides the appropriate basis for an improved thermodynamic interpretation of the Re(IV) solubility and hydrolysis under the investigated conditions. Considering ReO_2(s) as solid phase controlling the solubility (as is the case in the undersaturation experiments), and the slopes ≈ 0 and ≈ +1 (log [Re] *vs.* pH_m) identified from solubility data at pH_m below and above ≈10, respectively, the following equilibrium reactions can be defined:

$$ReO_2(s) + H_2O(l) \Leftrightarrow ReO(OH)_2(aq) \quad (2)$$

$$ReO_2(s) + 2H_2O(l) \Leftrightarrow ReO(OH)_3^- + H^+ \quad (3)$$

for which the corresponding conditional solubility constants (log $^*K'_{s,(1,x)}$, x 2–3 and I 0.1 M NaCl) and solubility constants at the reference state (log $^*K^\circ_{s,(1,x)}$, x 2–3 and I 0) are derived:

$$\log {}^*K'_{s,(1,2)} \quad \log [ReO(OH)_2(aq)] \quad (4)$$

$$\log {}^*K^\circ_{s,(1,2)} \quad \log {}^*K'_{s,(1,2)} \quad \log a_w \quad (5)$$

with a_w being the activity of water, and

$$\log {}^{*}K'_{s,(1,3)} \quad \log \left[\mathrm{ReO(OH)_3^-}\right] + \log[\mathrm{H^+}] \tag{6}$$

$$\log {}^{*}K^{\circ}_{s,(1,3)} \quad \log {}^{*}K'_{s,(1,3)} + \log \gamma \mathrm{ReO(OH)_3^-} + \log \gamma_{\mathrm{H^+}} \quad 2 \log a_w \tag{7}$$

Based on the fit of the experimental solubility data, the minimization of the function $\Sigma((\log [\mathrm{Re}]_{exp} - \log [\mathrm{Re}]_{calc})^2)^{1/2}$ was used to determine $\log {}^{*}K'_{s,(1,2)}$ –(6.3 ± 0.5) and $\log {}^{*}K'_{s,(1,3)}$ –(16.9 ± 0.4). The Specific Ion Interaction (SIT) theory as favored by the NEA-TDB (Grenthe et al., 2020) was used to calculate the activity coefficients $\log \log \gamma \mathrm{ReO(OH)_3^-}$ and $\log \gamma_{\mathrm{H^+}}$. Considering the specific ion interaction parameters $\varepsilon(\mathrm{ReO(OH)_3^-}, \mathrm{Na^+})$ $\varepsilon(\mathrm{TcO(OH)_3^-}, \mathrm{Na^+})$ –(0.08 ± 0.04) kg·mol^{-1}, $\varepsilon(\mathrm{H^+}, \mathrm{Cl^-})$ (0.12 ± 0.01) kg·mol^{-1} and $\log a_w$ (0.1 M NaCl) 0.0015 as reported in (Grenthe et al., 2020), the solubility constants in the reference state are calculated as $\log {}^{*}K^{\circ}_{s,(1,2)}$ –(6.3 ± 0.5) and $\log {}^{*}K^{\circ}_{s,(1,3)}$ –(17.1 ± 0.4). Note that these solubility constants are calculated assuming the anhydrous character of the ReO_2(s) solid phase, which was not confirmed by experimental means. However, the impact of $\log a_w$ on the calculation of $\log {}^{*}K^{\circ}_{s,(1,2)}$ and $\log {}^{*}K^{\circ}_{s,(1,3)}$ is clearly negligible for the low ionic strength conditions considered in the present study, *i.e.* 0.1 M NaCl. The uncertainty in the number of hydration waters of the solid phase is expected to become more relevant when investigating systems at high ionic strength conditions, *e.g.* 5.0 M NaCl.

Insights on the thermodynamics of Re(IV) hydrolysis can be gained through the combination of the solubility reactions (2) and (3):

$$\mathrm{ReO(OH)_2(aq) + H_2O(l) \Leftrightarrow ReO(OH)_3^- + H^+} \tag{8}$$

with $\log {}^{*}K^{\circ}_{(1,3)}$ $\log {}^{*}K^{\circ}_{s,(1,3)} - \log {}^{*}K^{\circ}_{s,(1,2)}$ –(10.8 ± 0.6). Solubility and hydrolysis constants determined in the present work are summarized in Table 1, which includes also thermodynamic data reported in the literature for Re(IV) and analogous Tc(IV) systems.

Table 1 shows that the solubility constant $\log {}^{*}K^{\circ}_{s,(1,2)}$ determined in this work for ReO_2(s). Due to the similar solubility data reported by Kim and Boulégue (Kim and Boulègue, 2003), we expected the solubility constants, calculated from this data, to be in good agreement. The value of $\log {}^{*}K^{\circ}_{s,(1,2)}$ determined from our solubility data at t 22 °C agrees within the uncertainties with the solubility constant calculated using the temperature function derived in Xiong et al. (2006) from solubility data at t 100–200 °C. Moreover, these values are in the same range (within the very large uncertainties) of the $\log {}^{*}K^{\circ}_{s,(1,2)}$ selected in the NEA-TDB for the precipitated Tc(IV) hydrous oxide, TcO_2(am, hyd). The hydrolysis constant $\log {}^{*}K^{\circ}_{(1,3)}$ determined in this work is almost three orders of magnitude higher than that estimated by Kim and Boulégue (Kim and Boulègue, 2003). As discussed in section 3.3, the experimental basis obtained by the latter authors (solubility data restricted to pH < 10) is clearly insufficient for an accurate determination of $\log {}^{*}K^{\circ}_{(1,3)}$. On the contrary, the $\log {}^{*}K^{\circ}_{(1,3)}$ value determined in this work for Re(IV) is in excellent agreement with the corresponding value for Tc(IV), as experimentally determined by Yalçıntaş et al. (2016) or selected in the NEA-TDB (Grenthe et al., 2020). This observation supports the analogies in the aquatic chemistry of Re and Tc in the oxidation state +IV, which can be explained by the similar ionic radii of both metal ions (r^{4+}_{Re} 0.63 Å, r^{4+}_{Tc} 0.65 Å, both with coordination number of 6 (Shannon, 1976)). No positively charged hydrolysis species of Re(IV) were identified in the present study. As discussed in section 3.3, solubility experiments at higher acidities and/or higher ionic strengths should be targeted in order to enhance the stability of this/these species and thus be able to characterize its/their thermodynamic properties. On the basis of the confirmed similarities in the aquatic chemistry of Re(IV) and Tc(IV), we propose the use of the equilibrium constant selected in the NEA-TDB for $Tc_2O_2(OH)_2^{2+}$ as tentative value for scoping calculations.

4. Summary and conclusions

The redox chemistry of Re(VII)/Re(IV) and the solubility and hydrolysis of Re(IV) were systematically investigated in reducing aqueous systems at 1 ≤ pH_m ≤ 12.8 and low ionic strength. Redox experiments were performed from oversaturation conditions with $[NaReO_4]_0$ 10^{-3} M, whereas solubility experiments were conducted from undersaturation conditions using commercial ReO_2(s).

Experimental (pe + pH_m) measurements in combination with thermodynamic equilibrium calculations (as *Pourbaix* diagrams) predict the predominance of Re(IV) both in redox and solubility experiments. In the redox experiments, the reduction of Re(VII) to Re(IV) with the consequent decrease in Re concentration is only observed at $pH_m \approx 1$ and ≈12.8. In analogy to previous studies with Re(VII) and Sn(II), we hypothesize that the decreased Re concentration observed at $pH_m \approx 1$ can be attributed to the coupling of the reduction process with the incorporation of Re^{4+} into the structure of the *in-situ* forming SnO_2(s) solid phase. A similar mechanism may apply at $pH_m \approx 12.8$. The slower or inexistent Re(VII) reduction observed at 3 ≤ pH_m ≤ 12 for up to 352 d can be explained by the slow reduction kinetics characterizing multi-electron transitions, as well as by the decreased concentration of Sn(II) in solution caused by the formation of the sparingly soluble SnO (cr). The significantly faster reduction previously reported for Tc(VII) under analogous reducing conditions is explained on the basis of the greater stability of Re(VII) compared to Tc(VII), which results in a greater driving force (expressed as Δpe $pe_{borderline} - pe_{experimental}$) for the reduction of the latter under the same conditions.

Undersaturation solubility experiments with ReO_2(s) show two well-defined regions corresponding to the predominance of the aqueous species $ReO(OH)_2$(aq) (pH ≤ 10) and $ReO(OH)_3^-$ (pH > 10). In combination with solid phase characterization, the evaluation of the solubility data allows deriving chemical and thermodynamic models and data that properly explain the Re(IV) solubility behavior determined in this work and available in the literature for dilute aqueous systems with 1 ≤ pH_m ≤ 12.8. Thermodynamic data determined in this study for the hydrolysis of Re(IV) are in excellent agreement with data available for Tc(IV), and represent a significant improvement with respect to previous studies available on the Re(IV) system.

Our results emphasize the chemical analogy of Re and Tc in the +IV oxidation state, which is rationalized by the very similar ionic radii of both metal ions (r^{4+}_{Re} 0.63 Å, r^{4+}_{Tc} 0.65 Å). However, these elements do show a remarkably different redox chemistry, both in terms of kinetics and thermodynamic stability. This effect is related to the increasing stability of the +VII oxidation state along the Group 7 of the periodic table, with Mn ≪ Tc < Re. For this reason, we conclude that the use of Re as inactive chemical analogue of Tc should be considered with much precaution, especially in systems involving redox transformations.

Declaration of competing interest

The authors declare that they have no known competing financial interests or personal relationships that could have appeared to influence the work reported in this paper.

Acknowledgements

This work was funded by the German Federal Ministry of Economics and Technology (BMWi) within the framework of the VESPA II project under the contract number 02 E 11607C. The research stay of S. Park at KIT–INE was partially funded through the Korea Nuclear International Cooperation Foundation (KONICOF) Nuclear Global Internship Program. Frank Geyer, Annika Fried and Cornelia Walschburger (all KIT–INE) are gratefully acknowledged for the ICP–MS and ICP–OES measurements. Ignasi Puigdomènech (SKB) is kindly acknowledged for fruitful discussions on the Re thermodynamics.

References

Altmaier, M., Metz, V., Neck, V., Müller, R., Fanghanel, Th, 2003. Solid-liquid equilibria of $Mg(OH)_2$(cr) and $Mg_2(OH)_3Cl{\cdot}4H_2O$(cr) in the system Mg-Na-H-OH-Cl-H_2O at 25°C. Geochem. Cosmochim. Acta 67, 3595–3601. https://doi.org/10.1016/S0016-7037(03)00165-0.

Anderson, C.D., Taylor, P.R., Anderson, C.G., 2013. Extractive metallurgy of rhenium: a review. Min. Metall. Explor. 30, 59–73. https://doi.org/10.1007/BF03402342.

Baumann, A., Yalçıntaş, E., Gaona, X., Altmaier, M., Geckeis, H., 2017. Solubility and hydrolysis of Tc(IV) in dilute to concentrated KCl solutions: an extended thermodynamic model for Tc^{4+}–H^+–K^+–Na^+–Mg^{2+}–Ca^{2+}–OH –Cl –H_2O(l) mixed systems. New J. Chem. 41, 9077–9086. https://doi.org/10.1039/C7NJ01116a.

Gamsjäger, H., Bugajda, T., Sangster, J., Saxena, S.K., Voigt, W., 2012. Chemical Thermodynamics of Tin. OECD Publications, Paris ; France.

Gates-Rector, S., Blanton, T., 2019. The Powder Diffraction File: a quality materials characterization database. Powder Diffr. 34, 352–360. https://doi.org/10.1017/S0885715619000812.

Grenthe, I., Gaona, X., Plyasunov, A.V., Linfeng, R., Runde, W.H., Grambow, B., Konings, R.J.M., 2020. In: Pu, Am, Tc (Eds.), Second Update on the Chemical Thermodynamics of U, Np. OECD Publications, Paris ; France.

Khan, M., Um, W., Kim, W.-S., Heo, J., Kim, H., Chang, S., 2018. Synthesis of rhenium-doped tin dioxide for technetium radioactive waste immobilization. J. Nucl. Mater. 505, 134–142. https://doi.org/10.1016/j.jnucmat.2018.04.014.

Kim, E., Boulègue, J., 2003. Chemistry of rhenium as an analogue of technetium: experimental studies of the dissolution of rhenium oxides in aqueous solutions. Radiochim. Acta 91, 211–216. https://doi.org/10.1524/ract.91.4.211.19968.

Kobayashi, T., Scheinost, A.C., Fellhauer, D., Gaona, X., Altmaier, M., 2013. Redox behavior of Tc(VII)/Tc(IV) under various reducing conditions in 0.1 M NaCl solutions. Radiochim. Acta 101, 323–332. https://doi.org/10.1524/ract.2013.2040.

Korzhinsky, M.A., Tkachenko, S.I., Shmulovich, K.I., Taran, Y.A., Steinberg, G.S., 1994. Discovery of a pure rhenium mineral at Kudriavy volcano. Nature 369, 51–52. https://doi.org/10.1038/369051a0.

Lukens, W.W., McKeown, D.A., Buechele, A.C., Muller, I.S., Shuh, D.K., Pegg, I.L., 2007. Dissimilar behavior of technetium and rhenium in borosilicate waste glass as determined by X-ray absorption spectroscopy. Chem. Mater. 19, 559–566. https://doi.org/10.1021/cm0622001.

Lwin, S., Wachs, I.E., 2014. Olefin metathesis by supported metal oxide catalysts. ACS Catal. 4, 2505–2520. https://doi.org/10.1021/cs500528h.

Magneli, A., 1957. Studies on rhenium oxides. Acta Chem. Scand. 11, 28–33.

Maset, E.R., Sidhu, S.H., Fisher, A., Heydon, A., Worsfold, P.J., Cartwright, A.J., Keith-Roach, M.J., 2006. Effect of organic Co-contaminants on technetium and rhenium speciation and solubility under reducing conditions. Environ. Sci. Technol. 40, 5472–5477. https://doi.org/10.1021/es061157f.

Maun, E.K., Davidson, N., 1950. Investigations in the chemistry of rhenium. I. Oxidation states IV, V and VII1,2. J. Am. Chem. Soc. 72, 2254–2260. https://doi.org/10.1021/ja01161a104.

Millensifer, T.A., 2010. Rhenium and rhenium compounds. In: Kirk-Othmer Encyclopedia of Chemical Technology. American Cancer Society, pp. 1–22. https://doi.org/10.1002/0471238961.1808051420180509.a01.pub3.

Mol, J.C., 1999. Olefin metathesis over supported rhenium oxide catalysts. Catal. Today 51, 289–299. https://doi.org/10.1016/S0920-5861(99)00051-6.

Naumov, A.V., 2007. Rhythms of rhenium. Russ. J. Non-Ferrous Metals 48, 418–423. https://doi.org/10.3103/S1067821207060089.

Poineau, F., Fattahi, M., Auwer, C.D., Hennig, C., Grambow, B., 2006. Speciation of technetium and rhenium complexes by in situ XAS-electrochemistry. Radiochim. Acta 94, 283–289. https://doi.org/10.1524/ract.2006.94.5.283.

Puigdomènech, I., Colàs, E., Grivé, M., Campos, I., García, D., 2014. A tool to draw chemical equilibrium diagrams using SIT: applications to geochemical systems and radionuclide solubility. MRS Online Proc. Libr. Arch. 1665, 111–116. https://doi.org/10.1557/opl.2014.635.

Rulfs, C.L., Meyer, R.J., 1955. Rhenium(IV) compounds: synthesis and properties. J. Am. Chem. Soc. 77, 4505–4507. https://doi.org/10.1021/ja01622a018.

Shannon, R.D., 1976. Revised effective ionic radii and systematic studies of interatomic distances in halides and chalcogenides. Acta Crystallogr. A 32, 751–767. https://doi.org/10.1107/S0567739476001551.

Tessalina, S.G., Yudovskaya, M.A., Chaplygin, I.V., Birck, J.L., Capmas, F., 2008. Sources of unique rhenium enrichment in fumaroles and sulphides at Kudryavy volcano. Geochem. Cosmochim. Acta 72, 889–909. https://doi.org/10.1016/j.gca.2007.11.015.

Wong-Ng, W., McMurdie, H.F., Hubbard, C.R., Mighell, A.D., 2001. JCPDS-ICDD research associateship (cooperative program with NBS/NIST). J. Res. Natl. Inst. Stand. Technol. 106, 1013–1028. https://doi.org/10.6028/jres.106.052.

Woolf, A.A., 1961. An outline of rhenium chemistry. Chem. Soc. Q. Rev. 15, 372–391.

Xiong, Y., Wood, S., 2001. Hydrothermal transport and deposition of rhenium under subcritical conditions (up to 200 C) in light of experimental studies. Econ. Geol. 96, 1429–1444. https://doi.org/10.2113/gsecongeo.96.6.1429.

Xiong, Y., Wood, S., Kruszewski, J., 2006. Hydrothermal transport and deposition of rhenium under subcritical conditions revisited. Econ. Geol. 101, 471–478. https://doi.org/10.2113/gsecongeo.101.2.471.

Xiong, Y., Wood, S.A., 1999. Experimental determination of the solubility of ReO_2 and the dominant oxidation state of rhenium in hydrothermal solutions. Chem. Geol. 158, 245–256. https://doi.org/10.1016/S0009-2541(99)00050-9.

Yalçıntaş, E., Gaona, X., Altmaier, M., Dardenne, K., Polly, R., Geckeis, H., 2016. Thermodynamic description of Tc(IV) solubility and hydrolysis in dilute to concentrated NaCl, $MgCl_2$ and $CaCl_2$ solutions. Dalton Trans. 45, 8916–8936. https://doi.org/10.1039/C6DT00973E.

Yalçıntaş, E., Gaona, X., Scheinost, A.C., Kobayashi, T., Altmaier, M., Geckeis, H., 2015. Redox chemistry of Tc(VII)/Tc(IV) in dilute to concentrated NaCl and $MgCl_2$ solutions. Radiochim. Acta 103, 57–72. https://doi.org/10.1515/ract-2014-2272.